Research Article



Adaptive set point modulation to mitigate transients in power systems

ISSN 1751-8687 Received on 30th September 2019 Revised 21st July 2020 Accepted on 18th August 2020 E-First on 14th October 2020 doi: 10.1049/iet-gtd.2019.1455 www.ietdl.org

Hooman Ghaffarzadeh¹ ⋈, Ali Mehrizi-Sani²

¹School of Electrical Engineering and Computer Science, Washington State University, 355 Spokane Street, Pullman, WA, USA ²Bradley Department of Electrical and Computer Engineering, Virginia Polytechnic Institute and State University, Blacksburg, VA, USA

⊠ E-mail: hooman.ghaffarzadeh@wsu.edu

Abstract: This paper presents an adaptive control strategy to improve the transient response of a stressed power system apparatus. This strategy, based on the set point automatic adjustment with correction-enabled (SPAACE), is an auxiliary control method to enhance the set point tracking of an apparatus. SPAACE modifies the set point of the controllable apparatus using a feedback signal from its output to mitigate transients that can be caused by events such as faults, load variations, and large reference set point changes. In this work, an adaptive version of SPAACE (ASPAACE), which uses an adaptive dead-zone band, adaptive scaling factor, and exponential prediction is introduced. Moreover, this study investigates the relationship between the natural frequency of the system and the prediction horizon of the ASPAACE controller. To demonstrate the performance of ASPAACE, different case studies are presented.

1 Introduction

In recent years, increased penetration of distributed energy resources (DERs) without rotational inertia have introduced new operational challenges for grid operators. Moreover, the grid codes and IEEE standards, such as IEEE P2800 (standard for interconnection and interoperability of inverter-based resources interconnecting with associated transmission electric power systems) and IEEE 1547.2018 (standard on smart inverters) recommend and mandate the grid operators with different rules for the integration of the inverter-based resources into the grid. Furthermore, large variations in the generation-load profile and structure of the power system can deteriorate the stability of the system. DERs typically use renewable energy resources such as solar panels, wind turbines, and small hydroelectric plants, and they typically require a power electronic-based interface to connect to the grid. Therefore, in comparison with conventional power generators, DERs are more flexible from control aspects [1]. However, because of lack of rotational inertia, DERs are more vulnerable to the transients caused by faults and load variations that can cause instability, tripping of protective devices, or violation of the ratings of apparatuses [2-5]. The conventional fixed-parameters control techniques cannot necessarily ensure the transient stability of the system. Therefore, new approaches need to be developed to improve the damping of a system under varying operating conditions [6].

To address the aforementioned challenges, several strategies are introduced in the literature. To improve the voltage and power dynamics of an inverter-based DER unit, a robust H_{∞} controller is proposed in [7]. An equivalent model using a microgrid dynamic equivalent circuit including uncertainties coming from microgrid impedance variation is developed to design a robust H_{∞} voltage controller. Similarly, Davari and Mohamed [8] introduced a robust disturbance rejection controller based on the singular-values μ synthesis approach to control a voltage-sourced converter (VSC) under a wide range of operating conditions. The proposed methods in [7, 8] can improve the dynamic stability of DER units under a wide range of operating conditions; however, they are complicated and hard to realise. Leon et al. [9] proposed an adaptive controller for an HVDC system under balanced and unbalanced network conditions. In this approach, a resonant filter is used to eliminate the double-frequency ripple on the DC side voltage of the VSC. However, adding a filter to the control loop of a VSC negatively

affects the controller performance by introducing a delay. Liu and Hsu [10] utilised the particle swarm optimisation (PSO) algorithm to propose a self-tuning PI controller for a static synchronous compensator (STATCOM). In this method, using the estimated load impedance information from real-time measurements of the system, the coefficients of the PI controller are tuned. A real-time method for optimal tuning of the gains of a PI controller in a microgrid using fuzzy logic and PSO algorithm is proposed in [11]. Hasanien and Matar [12] proposed a fuzzy logic controller to control the real and reactive power a VSC-based DER under the islanded mode of operation. A self-tuning fuzzy critic-based method is proposed in [1]. In this approach, a neurodynamic programming technique is utilised to adjust the parameters of the controller. In [13], an optimisation-based algorithm is introduced to obtain the optimal coefficients of the PI controllers of a VSC under dq-current control. In this approach, a constrained convex optimisation problem is solved to shape the trajectory of the closed-loop and open-loop transfer matrices of the system. However, the methods proposed in [1, 10–14] need a significant computational power. In [15], a tuning approach is proposed to modify the parameters of PI controllers of a converter in a gridconnected wind turbine. This approach is based on linear control for multivariable systems and it needs an accurate model of the plant. Chen et al. [16] proposed a control method to adjust the real and reactive power injection of an electric spring to mitigate the frequency and voltage fluctuations in a wind system. The proposed controller adjusts the amplitude and the shift angle of the modulation signal in the electric spring. An adaptive voltage control approach to improve the dynamic stability of DER units using a PI feedback controller is proposed in [17]. In this approach, the parameters of the PI controller are dynamically adjusted to respond to system changes. However, the need for a priori knowledge of the system, which is not usually available, and lack of robustness to changes in the system parameters are the main drawbacks of the proposed approaches in [15–17].

To address the disadvantages of the previously proposed approaches, a controller called SPAACE (set point automatic adjustment with correction enabled) is proposed in [6, 18–21]. SPAACE is an autonomous auxiliary controller that operates between the secondary and primary controllers of an apparatus (see Fig. 1). SPAACE monitors the variable of interest in an apparatus and based on its trend and operational limits, modifies the set point to improve its dynamic performance. To enhance the performance

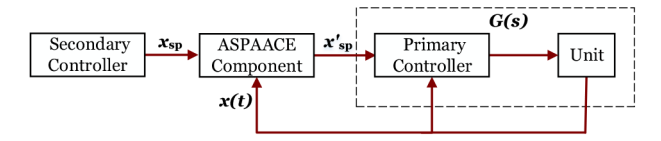


Fig. 1 Schematic diagram of SPAACE between the primary and secondary controllers

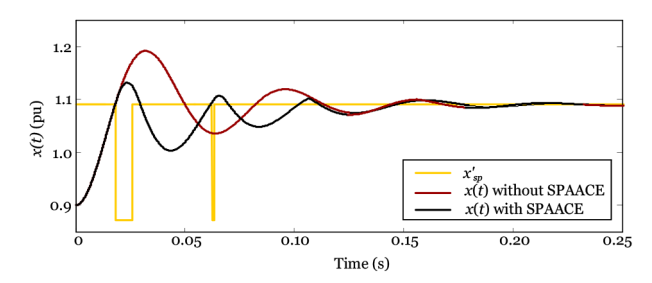


Fig. 2 Example implementation of SPAACE

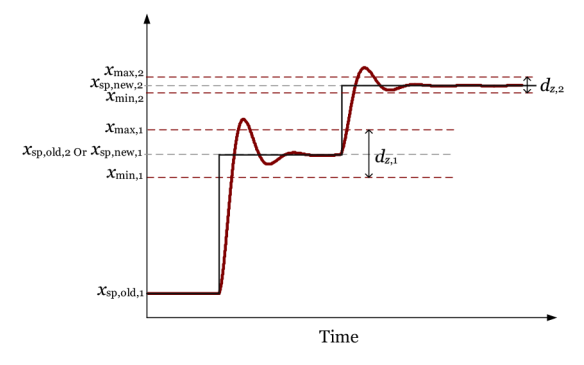


Fig. 3 Adaptive dead-zone band

of SPAACE, an adaptive variant of SPAACE (ASPAACE) is proposed in this paper. The main contributions of this work are as follows:

- An adaptive dead-zone band and adaptive scaling factor for ASPAACE to enhance its tracking performance.
- A prediction algorithm using exponential extrapolation to improve prediction accuracy.
- A study to investigate the relationship between the natural frequency of the system and the prediction horizon.
- A discussion to prove the existence of a smooth response for a third-order dynamic system with ASPAACE.

This paper is organised as follows. In Section 2, the original version of SPAACE with prediction is reviewed. In Section 3, the proposed ASPAACE controller is introduced and a new prediction approach is proposed. Section 4 discusses the proof of existence of a smooth response for a third-order system with ASPAACE. In Section 5, the performance of ASPAACE under different scenarios is evaluated and the relationship between the prediction horizon of ASPAACE and the natural frequency of a system is analysed. Section 6 concludes the paper.

2 Introduction to the SPAACE controller

2.1 Preliminaries

SPAACE as a supplementary controller can be added to the existing controllers of an apparatus to keep its response x(t) within its maximum x_{\max} and minimum x_{\min} allowable limits. SPAACE, based on trend of x(t), modifies the reference set point of the apparatus to mitigate the response overshoot when the output signal violates the limits.

An example of SPAACE implementation is shown in Fig. 2. In this case, the reference set point of an apparatus is changed in a step from 0.90 to 1.09 pu at t = 0. Once the output signal passes

 x_{max} (in this example, 1.10 pu), SPAACE scales down the set point to mitigate the overshoot.

2.2 SPAACE with prediction

SPAACE with prediction is introduced in [19] to increase the reaction speed of SPAACE. The original SPAACE controller (i.e. without prediction) only uses the real-time value of the signal of interest x(t). However, SPAACE with prediction uses the real-time and past sampled values of x(t) to predict its future values.

A linear extrapolation approach is used in [19] to calculate the predicted value. The values of $x(t_0)$ and $x(t_0 - T_{past})$ are used to calculate the average rate of changes of x(t) and $x(t_0 + T_{pred})$, where T_{past} is the value of the x(t) in n past sampling time, t_0 is the current time, and T_{pred} is the prediction horizon. r is the average rate of change of x(t) between $t_0 - T_{past}$ and t_0 [18–20]. T_{past} and r are defined as

$$T_{\text{past}} = nT_{\text{s}},\tag{1}$$

$$r = \frac{x(t_0) - x(t_0 - T_{\text{past}})}{T_{\text{past}}},$$
 (2)

where T_s is the sampling time. $x(t_0 + T_{pred})$ is calculated as

$$x(t_0 + T_{\text{pred}}) = x(t_0) + rT_{\text{pred}}.$$
 (3)

The prediction-enabled SPAACE adjusts the set point as [6]

$$x_{\text{sp}}' = \begin{cases} (1-m)x_{\text{sp}}, & x(t_0 + T_{\text{pred}}) > x_{\text{max}} \text{ and } x_{\text{sp}} > 0, \text{ or} \\ & x(t_0 + T_{\text{pred}}) < x_{\text{min}} \text{ and } x_{\text{sp}} < 0 \\ (1+m)x_{\text{sp}}, & x(t_0 + T_{\text{pred}}) < x_{\text{min}} \text{ and } x_{\text{sp}} > 0, \text{ or} \\ & x(t_0 + T_{\text{pred}}) > x_{\text{max}} \text{ and } x_{\text{sp}} < 0 \\ x_{\text{sp}}, & \text{otherwise}, \end{cases}$$
(4)

where x_{sp} is the reference set point of the apparatus and m is a heuristically predetermined scaling factor [22, 23].

3 Adaptive SPAACE

In this paper, an adaptive version of SPAACE (ASPAACE) is proposed. In this approach, the scaling factor and the dead-zone band (a virtual band around the reference set point defined in the next subsection) change based on the magnitude of the change in the reference set point. Moreover, a new prediction approach using the exponential extrapolation is introduced to further improve the tracking performance of ASPAACE.

3.1 Adaptive dead-zone band

The original SPAACE controller proposed in [18, 19] only responds to the transients that violate the operational limits of the controlled apparatus. Ghaffarzadeh *et al.* [6] introduced the concept of the dead-zone band as a virtual band around the reference set point of the controlled apparatus to further improve the tracking performance of SPAACE by mitigating the transients even when they stay within the operational limits of the apparatus. The size of the dead-zone band introduced in [6] depends only on the current value of the reference set point.

This paper proposes an adaptive dead-zone band for ASPAACE based on the magnitude of the change in the reference set point, as shown in Fig. 3

$$d_{\rm z} = \Delta x_{\rm sp} S_{\rm d},\tag{5}$$

where d_z is the width of dead-zone band and S_d is a heuristically chosen factor determined based on the desired response quality (e.g. for a response with a big signal-to-noise ratio (SNR), a smaller S_d should be selected). $\Delta x_{\rm sp}$ is the magnitude of the change in $x_{\rm sp}$:

$$\Delta x_{\rm sp} = |x_{\rm sp,old} - x_{\rm sp,new}|. \tag{6}$$

ASPAACE adaptively shrinks the operational limits to a band around the set point, separated by a distance d_z . The maximum and minimum operational limits are defined as

$$x_{\text{max}} = x_{\text{sp}} + \frac{d_{\text{z}}}{2},$$

$$x_{\text{min}} = x_{\text{sp}} - \frac{d_{\text{z}}}{2}.$$
(7)

3.2 Adaptive scaling factor

ASPAACE also uses an adaptive scaling factor. In ASPAACE, unlike the original algorithm, the value of the scaling variable adaptively changes with the magnitude of the reference set point. Fig. 4 shows the concept of adaptive scaling factor m' calculated as

$$m' = \Delta x_{\rm sp} m \,. \tag{8}$$

Adaptive dead-zone band and scaling factor only operate in the cases that the reference set point of a controlled apparatus is changed. For the transients caused by an external factor (e.g. faults) that the reference set point is constant, the original dead-zone band and scaling factor are used.

3.3 Exponential prediction

To further increase the reaction speed of ASPAACE and improve its tracking performance, this paper uses exponential extrapolation to predict the response of the controlled apparatus. The following exponential function is considered

$$x(t) = ae^{bt}, (9)$$

where a and b are two constants determined by a linear regression method. By taking the natural logarithm from both sides of (9), a linear equation can be derived as

$$y(t) = c + bt, (10)$$

where a, b, and c can be calculated as

$$a = e^c, (11)$$

$$b = \frac{n(\sum_{i=-n+1}^{0} t_i y(t_i)) - (\sum_{i=-n+1}^{0} t_i)(\sum_{i=-n+1}^{0} y(t_i))}{-(\sum_{i=-n+1}^{0} t_i)^2},$$
 (12)

$$c = \frac{\left(\sum_{i=-n+1}^{0} y(t_i)\right) - b\left(\sum_{i=-n+1}^{0} t_i\right)}{n},$$
(13)

where n is the number of the past stored sampling points. The predicted value of x(t) can be calculated from

$$\hat{x}(t_0 + T_{\text{pred}}) = ae^{b(t_0 + T_{\text{pred}})}.$$
 (14)

4 Existence of a smooth response

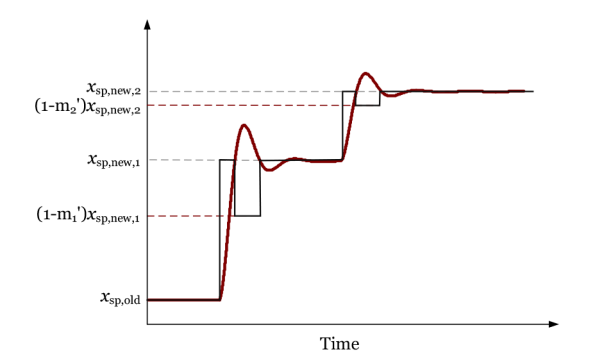


Fig. 4 Adaptive scaling factor

Mehrizi-Sani and Iravani [19] discussed the existence of a smooth response (i.e. response with smaller over/undershoot and shorter settling time than the system base response without SPAACE) with an appropriate selection of time instances to modify the reference set point by the SPAACE controller. Fig. 5 shows this concept, where T_1 and T_2 are the time instances that the set point switches between the original and the modified values. This approach can be summarised as follows:

- Select T_1 such that $x_p = 1$; and
- Calculate time t_p (when the maximum overshoot happens) and select T_2 to be equal to t_p .

The peak time and the overshoot of the response of an underdamped (0 < ζ < 1) second-order system are

$$t_{\rm p} = \frac{\pi}{\omega_n \sqrt{1 - \zeta^2}},\tag{15}$$

$$M_{\rm p} = e^{\frac{-\zeta\pi}{\sqrt{1-\zeta^2}}} \times 100. \tag{16}$$

Equations (15) and (16) are valid only for a second-order system. However, the second-order representation is generally not sufficient to characterise the response of a system. Thus, a third- or higher-order transfer function is used to represent the dynamics of the study system. However, designing a controller for such higher-order systems is not straightforward. Therefore, their behaviour is approximated with a combination of first- and second-order systems using the dominant pole approximation approach [24].

In this paper, the behaviour of a third-order system with the ASPAACE controller in response to changes in the set point is studied. In (17), G(s) represents the transfer function of a third-order system [25]

$$G(s) = \frac{\omega_n^2 P}{(s^2 + 2\zeta \omega_n s + \omega_n)(s + P)},$$
(17)

with a damping factor ζ , natural frequency ω_n , and a real pole at s=-P. The step response of G(s) has two components: (i) an oscillatory response due to the two complex conjugate poles at $s=-\zeta\omega_n\pm j\omega_n\sqrt{1-\zeta^2}$ and (ii) an exponentially decaying response due to the real pole at s=-P.

Based on the dominant pole approximation approach for an underdamped system [24], the following cases are considered. First, when the pole at s=-P is very close to the origin (i.e. $P \rightarrow 0$), it shapes the transient response of the system and the effect of the two complex poles diminishes. Therefore, the behaviour of the system can be described as

$$\tilde{G}(s) \simeq \frac{P}{s+P}, \quad P \ll \zeta \omega_n.$$
 (18)

Second, when the pole at s = -P is placed at least five times farther from the origin to the left than the complex poles, it can be neglected and the system can be approximated as an underdamped second-order system as

$$\tilde{G}(s) \simeq \frac{\omega_n^2}{s^2 + 2\zeta\omega_n s + \omega_n^2}, \quad P \gg \zeta\omega_n.$$
 (19)

Third, when P is comparable to $\zeta \omega_n$, the behaviour of the system is between a first- and a second-order systems from the settling time and the maximum peak value standpoints. Therefore, the effects of a single pole at s=-P on the step response of a third-order system compared with a second-order system are

- Decreasing the response overshoot.
- Increasing the settling time.

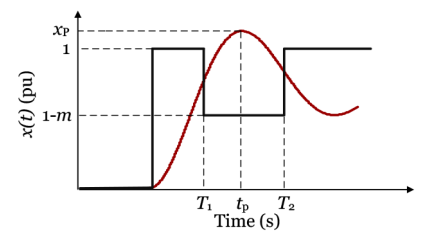


Fig. 5 Definition of t_p , T_1 , and T_2

To cover the three aforementioned conditions, Fig. 6 compares the step response of a third-order system with a single pole at s=-10, s=-50, or s=-500 with a second-order system with $\omega_n=82$ and $\zeta=0.21$ ($s=-17.22\pm j80.17$).

It can be seen that depending on the location of the single pole, the third-order system has a similar or smaller overshoot and settling time compared with a second-order system. Therefore, using the proposed approach in [19], as discussed at the beginning of this section, with an appropriate selection of the time instances for the reference set point changes, ASPAACE can provide a smooth response with shorter settling time and smaller peak value than the base system response without ASPAACE.

5 Performance evaluation

In this section, the performance of the proposed strategies in different case studies is evaluated using the PSCAD/EMTDC and MATLAB software environments. For the PSCAD/EMTDC simulations, the ASPAACE controller is programmed in FORTRAN and implemented as a user-defined component.

5.1 Relationship between the natural frequency of the system and the prediction horizon

In this subsection, using MATLAB software, the relationship between the natural frequency of a system and the prediction horizon of ASPAACE with linear prediction is studied. To this end, two second-order systems with $\zeta=0.1$ (Fig. 7a) and $\zeta=0.2$ (Fig. 7b) with varying ω_n are considered and a step change from 0.9 to 1.1 pu is applied to the reference set point at t=0 s. The scaling factor m is chosen to be 0.2. x_{\max} , x_{\min} , and d_z are 1.1, 0.9, and 0.04 pu, respectively. In Fig. 7, the minimum peak value for each case is indicated with a black asterisk. Based on Fig. 7, ω_n and T_{pred} have an inverse relationship such that as ω_n increases, the peak of the response occurs at a smaller T_{pred} . Therefore, for a system with a higher ω_n a smaller T_{pred} should be selected.

5.2 ASPAACE with exponential prediction

In this case study, for a second-order system with $\zeta=0.4$ and $\omega_n=82$, a step change from 0 to 1 pu is applied at $t=0\,\mathrm{s}$. The scaling factor m is heuristically chosen to be 0.5 and the sampling time T_s is set to 1 ms. T_past and T_pred are set to 4 and 7 ms, respectively. x_max , x_min , and d_z are 1.1, 0.9, and 0.04 pu, respectively. Fig. 8a shows the response of x(t) with ASPAACE with linear prediction. The response without ASPAACE peaks at 1.75 pu and settles after 430 ms while the response with ASPAACE with linear prediction peaks at 1.22 pu (30% improvement) and settles after 62 ms (85% improvement). Fig. 8b shows the response of system with ASPAACE with exponential prediction. ASPAACE with exponential prediction. ASPAACE with no overshoot.

5.3 Balanced network condition

To evaluate the performance of ASPAACE under balanced load condition, the control method based on the sequential loop closing (SLC) approach introduced in [26] is utilised. In the SLC method, a system with multiple inputs and outputs is divided into several most related single-input single-output (SISO) systems and a controller is designed for each [26]. This process will continue for

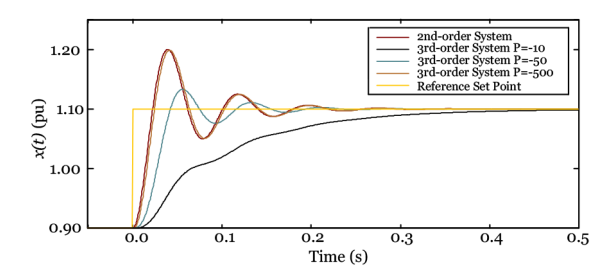


Fig. 6 Comparison between the step response of a third-order system with a single pole at s = -10, s = -50, or s = -500 with a second-order system

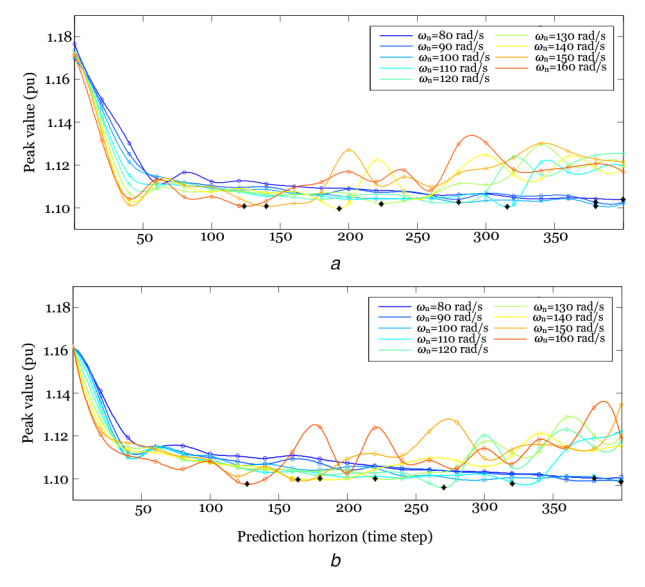


Fig. 7 Relationship between the peak value and the corresponding T_{pred} for systems with different ω_n values

(a) $\zeta = 0.1$, (b) $\zeta = 0.2$

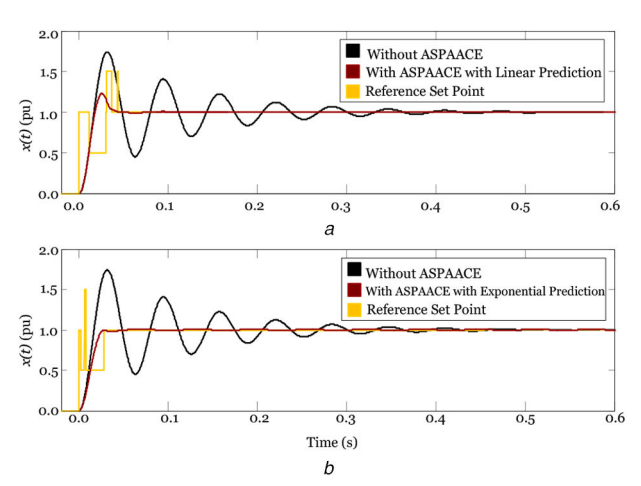


Fig. 8 *Response to a step change from 0 to 1 pu at t* = 0 s *(a)* With ASPAACE with linear prediction, *(b)* With ASPAACE with exponential prediction

other input—output variables pairs in the system by considering the previously designed controller as an integral part of the system. In this section, p(t) and q(t) (i.e. the instantaneous real and reactive powers) are used as the control variables.

The real and reactive powers of the VSC are controlled using an inner control loop, and the DC-side voltage of the VSC is controlled using an outer control loop. Fig. 9 shows the schematic diagram of the inner and outer control loops including the ASPAACE controllers. In Fig. 9, G(s) and $G_{\rm DC}(s)$ represent the dynamics of the controlled apparatus and the VSC DC-link, respectively. $C_{\rm inner,p}$ ($K_{\rm p}=0.000825$ and $K_{\rm i}=0.24$) and $C_{\rm inner,q}$ ($K_{\rm p}=0.00085$ and $K_{\rm i}=1$) are the PI controllers for the real and

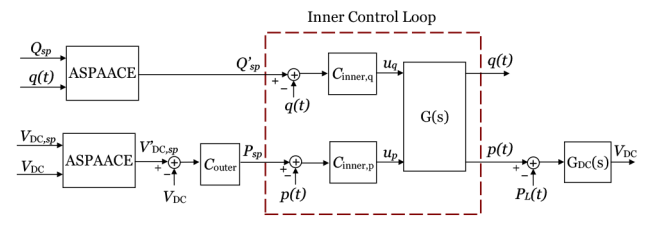


Fig. 9 Schematic diagram of the inner and outer control loops including the ASPAACE auxiliary controllers

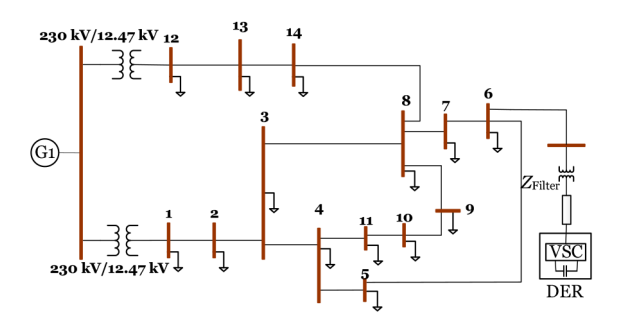


Fig. 10 One-line diagram of the 14-bus CIGRE North American feeder system augmented with a DER unit at bus 6

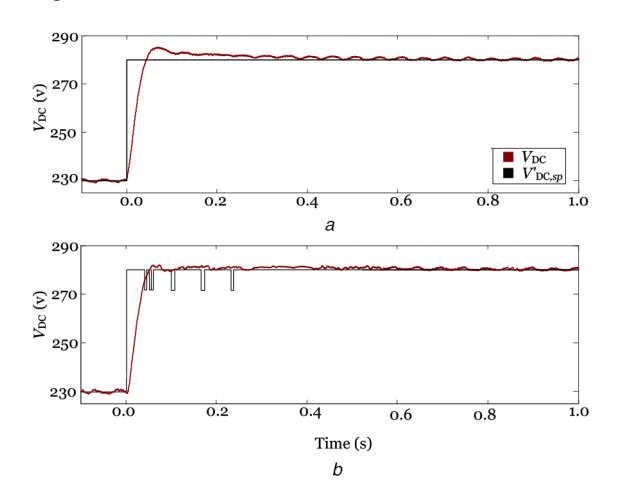


Fig. 11 *DC voltage response to a step change in its reference set point* (a) Without ASPAACE, (b) With ASPAACE

reactive powers designed using the SLC method. $C_{\rm outer}$ ($K_{\rm p}=60$ and $K_{\rm i}=200$) is the VSC DC-side voltage controller. Two separate ASPAACE controllers provide two separate reference set points for the reactive power controller ($Q_{\rm sp}$) and the DC-side voltage controller ($V_{\rm DC\ sp}$).

Fig. 10 shows the one-line diagram of the study system as the 14-bus CIGRE North American medium-voltage feeder system augmented with a DER unit at bus 6 [27]. To assess the performance of ASPAACE under balanced condition, the line parameters are averaged and the single-phase loads are replaced with the equivalent three-phase loads. The rated voltage of the grid (an ideal voltage source G1) is 230 kV and the rated voltage of the distribution level is 12.47 kV, which is stepped up using a 230 kV/ 12.47 kV transformer. The DER unit (a 230 V DC source, e.g. a regulated PV array) is integrated into the grid at bus 6 using a $12.47 \, \text{kV}/480 \, \text{V}$ transformer with an impedance Z_{Filter} of 0.02 + j0.10 pu (combination of the transformer impedance and an RL filter), with $S_{\text{base}} = 2$ MVA. A VSC operating at a switching frequency of 1620 Hz connects the DER unit to the power system. T_s (sampling time) is set to $5 \mu s$. The scaling factor m is heuristically chosen to be 0.1. T_{pred} and T_{past} are set to 7 ms. x_{max} , x_{\min} , and d_z are 1.1, 0.9, and 0.04 pu, respectively.

5.3.1 Step change in $V_{\rm DC}$ set point: In this case study, the DC voltage $V_{\rm DC}$ response to a step change in its reference set point from 230 to 280 V is presented.

The response of $V_{\rm DC}$ without ASPAACE intervention is shown in Fig. 11a. The response settles after 520 ms and peaks at 285 V. Fig. 11b shows the response with ASPAACE with exponential prediction. In the case with the ASPAACE controller, the response settling time is reduced to 62.4 ms (88% improvement) and the peak value is reduced to 281 V.

5.3.2 Step change in reactive power set point: In this case study, the performance of the system to a step change in the reference set point of q(t) is assessed. Initially, V_{DC} and Q_{sp} are set to 230 V and 1.0 MVAr, respectively. $Q_{\rm sp}$ is changed in a step to 2.5 MVAr at t = 0 s. To improve the reference tracking of V_{DC} and q(t)controllers, two separate ASPAACE components are employed. Figs. 12a and c show the response of DC voltage without and with ASPAACE. The response of V_{DC} is within the operational limits of the system; therefore, ASPAACE does not change the reference set point. The response of reactive power without ASPAACE intervention is shown in Fig. 12b. The response settles after 210 ms and peaks at 218 V. Fig. 12d shows the response with ASPAACE with exponential prediction. In the case with the ASPAACE controller, the response settling time is reduced to 121 ms (42% $\,$ improvement) over the base case response and without any considerable undershoot.

5.4 Unbalanced network condition

In this subsection, the original values of the line parameters and the loads of the study system in the previous subsection are used to evaluate the performance of ASPAACE with exponential prediction in an unbalanced network condition. The control is performed in the dq-frame and separate ASPAACE controllers are used to control the positive- and negative-sequences of the dq components of the variable of interest [6]. ASPAACE controllers provide individual reference set points for each of the mentioned components (see Fig. 13). The parameters of the PI controller that regulate i_d and i_q values are chosen to create a lightly damped system ($K_p = 0.05$ and $K_i = 20$). The sampling time T_s is set to 5 μ s. The scaling factor m is heuristically chosen to be 0.3. T_{pred} and T_{past} are set to 0.1 ms. x_{max} , x_{min} , and d_z are 1.1, 0.9, and 0.04 pu, respectively.

5.4.1 Step change in i_d^+ set point: In this case study, the positive component of i_d is set to 0.5 pu, the positive component of i_q and the negative component of i_d are set to 0.1 pu, and the negative component of i_q is set to 0 pu. A step change in i_d^+ from 0.5 to 1.2 pu is applied at t=0 s. The response of i_d^+ without ASPAACE intervention is shown in Fig. 14a. It settles after 180 ms and peaks at 1.59 pu. Figs. 14b and c show the response of system with SPAACE with linear prediction and ASPAACE with exponential prediction, respectively. In the case with SPAACE, the response settling time is reduced to 1.5 ms (36% improvement) and its peak value is reduced to 1.41 pu (11% improvement). In the case with ASPAACE, the response settling time is reduced to 73 ms (59% improvement) and its peak value is reduced to 1.3 pu (18% improvement).

5.4.2 Single-phase to ground fault: In this case study, a single-phase to ground fault is applied at time t = 0 s for 0.1 s and the behaviour of system under fault condition is evaluated. i_d^+ and i_d^- are set to 0.8 and 0.1 pu, respectively, and i_d^+ and i_d^- are set to 0 pu. The

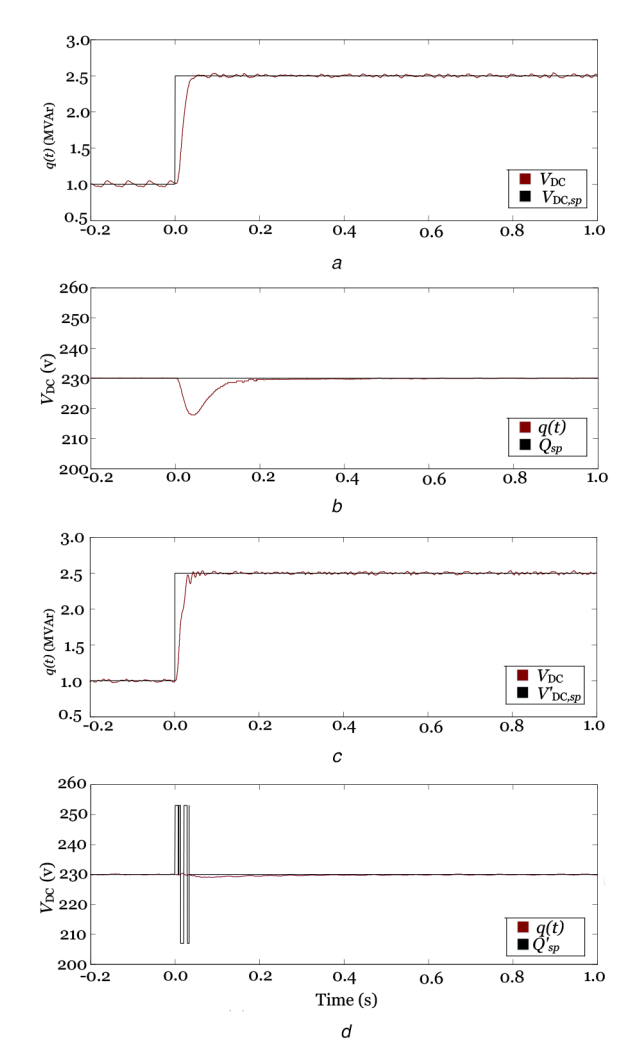


Fig. 12 V_{DC} and q(t) responses to a step change in the reference set point of the reactive power

(a) Reactive power without ASPAACE, (b) DC voltage without ASPAACE, (c) Reactive power with ASPAACE, (d) DC voltage with ASPAACE

response of i_d^+ without ASPAACE intervention is shown in Fig. 15a. It peaks at 1.19 pu and settles after 250 ms. Fig. 15b shows the response of system with ASPAACE with exponential prediction. In the case with ASPAACE, the response settling time is reduced to 210 ms (16% improvement) and its peak value is reduced to 1.08 pu (9% improvement) and unlike the case without ASPAACE, the response is smooth and does not significantly oscillate around the reference set point.

5.4.3 Multiple step changes in i_d^+ set point: In this case study, the positive and the negative components of i_d and i_q are set to 0 pu. At t=0 s, i_d^+ is changed in a step from 0 to 0.8 pu and at t=0.5 s it is changed to 1.2 pu. The response of i_d^+ without ASPAACE is shown in Fig. 16a.

It peaks at 1.2 and 1.4 pu, and settles after 150 and 105 ms for the first and second step changes, respectively. Figs. 16b and c show the response of system with SPAACE with linear prediction and ASPAACE with exponential prediction, respectively. For the first step change, the SPAACE response settling time is reduced to 100 ms (33% improvement) and its peak value is reduced to 1 pu (16% improvement). In the case with ASPAACE, the response settling time is reduced to 81 ms (46% improvement) and its peak value is reduced to 0.9 pu (25% improvement). For the second step change, the ASPPACE response settling time is reduced to 45 ms (70% improvement) and it is smooth and does not significantly oscillate around the reference set point compared with the case with the SPAACE controller.

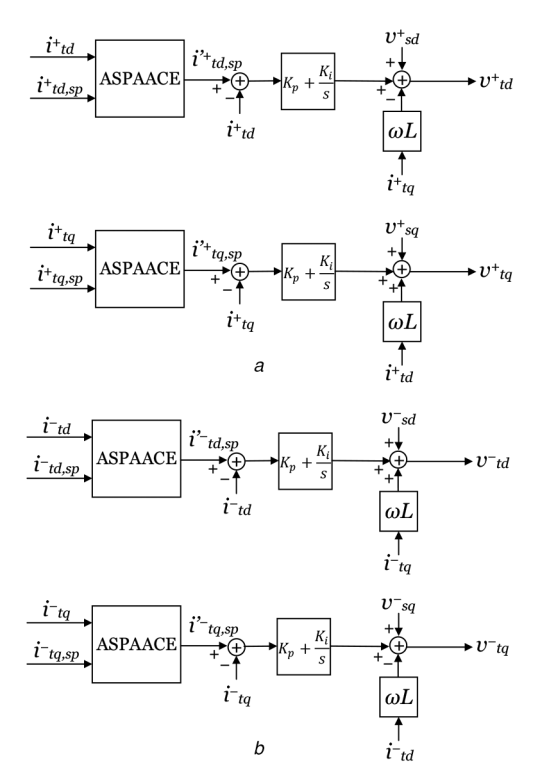


Fig. 13 Schematic diagram of the sequence network controllers in the deframe

(a) Positive sequence, (b) Negative sequence

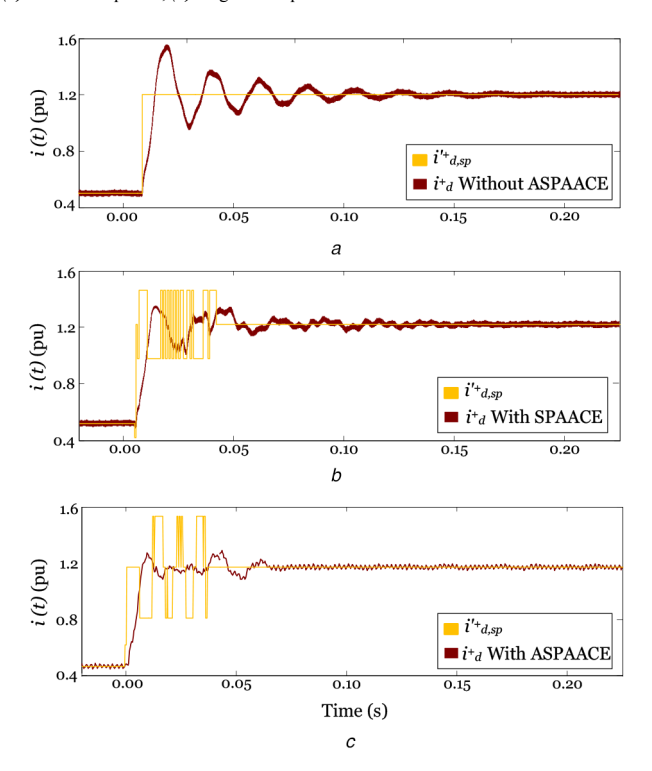


Fig. 14 Response to a step change in i_d^+ from 0.5 to 1.2 pu (a) Without ASPAACE, (b) With SPAACE with linear prediction, (c) With ASPAACE with exponential prediction

5.4.4 Step change in i_d^+ set point with a weak grid: In this case study, to analyse the performance of ASPAACE under weak grid conditions, the ideal voltage source G1 in Fig. 10 is replaced with a voltage source with a short-circuit ratio (SCR) of 3 and X/R of 10. The positive component of i_d is set to 1 pu, and the positive component of i_q , the negative component of i_d , and the negative component of i_q are set to 0 pu. A downward step change in i_d^+ from 1 to 0.5 pu is applied at t = 0.5 s. The response of i_d^+ without

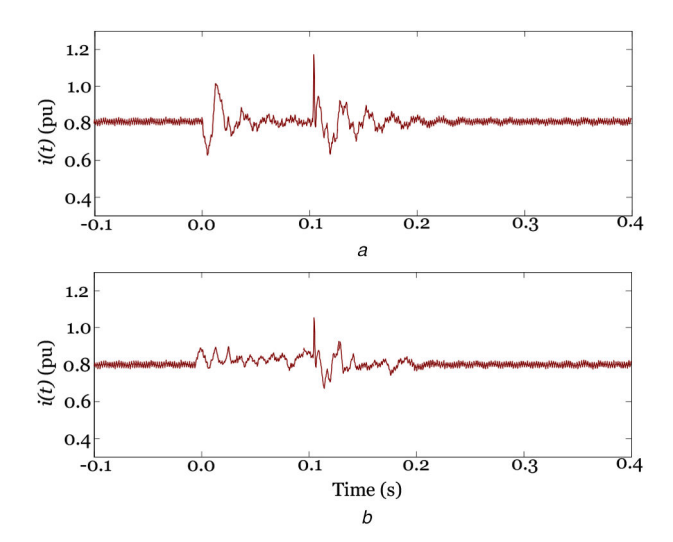


Fig. 15 Responses to a single-phase to ground fault at t = 0 s and cleared after 0.1 s

(a) Without ASPAACE, (b) With ASPAACE with exponential prediction

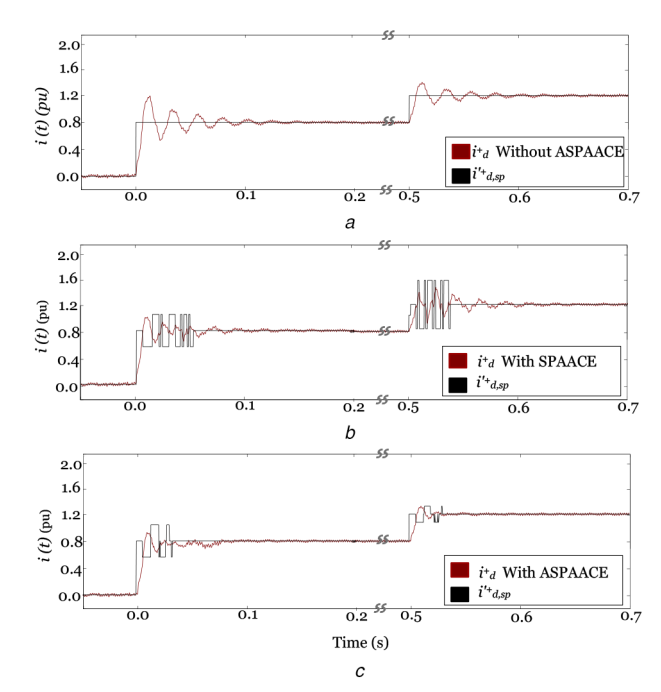


Fig. 16 Response to a step change in i_d^+ from 0 to 0.8 pu at t = 0 s and from 0.8 to 1.2 pu at t = 1.5 s

(a) Without ASPAACE, (b) With SPAACE, (c) With ASPAACE

ASPAACE intervention is shown in Fig. 17a. It settles after 160 ms with an undershoot of 44%. Fig. 17b shows the response of system with ASPAACE with exponential prediction. In this case, the response settling time is reduced to 120 ms (25% improvement) with an undershoot of 20% (22% improvement).

6 Conclusion

In this paper, an enhanced version of SPAACE called adaptive SPAACE (ASPAACE) is introduced. ASPAACE uses an adaptive scaling factor and dead-zone band to improve set point tracking of a controllable apparatus. Using the exponential extrapolation approach, a new prediction technique is introduced to improve the reaction speed of ASPAACE. Moreover, the relationship between the natural frequency of a system and the prediction horizon of ASPAACE with linear prediction is studied. In order to evaluate the performance of the proposed strategies, different case studies are conducted in the PSCAD/EMTDC and MATLAB software tools. The simulation results show that ASPAACE with exponential prediction is able to reduce peaks in the transient response and shorten violation times compared to linear prediction.

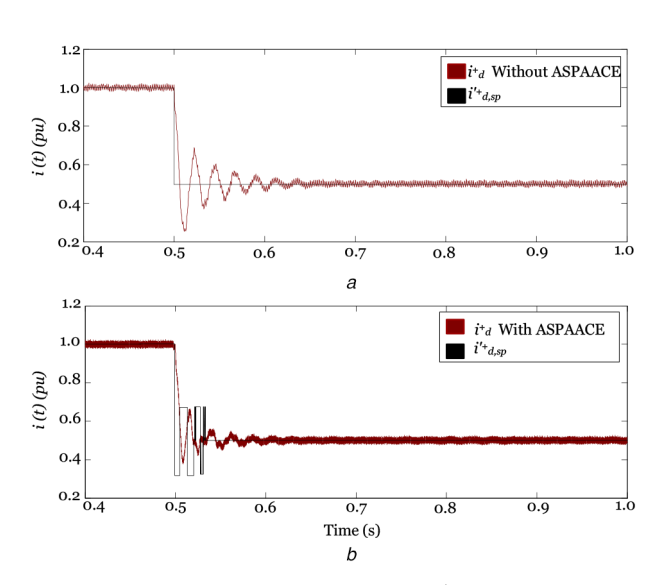


Fig. 17 Response to a downward step change in i_d^+ from 1 to 0.5 pu (a) Without ASPAACE, (b) With ASPAACE with exponential prediction

7 References

- Seidi-Khorramabadi, S., Bakhshi, A.: 'Critic-based self-tuning PI structure for active and reactive power control of VSCs in microgrid systems', *IEEE Trans. Smart Grid*, 2015, 6, (1), pp. 92–103
- [2] Benidris, M., Mitra, J.: 'Enhancing stability performance of renewable energy generators by utilizing virtual inertia'. IEEE Power Eng. Soc. General Meeting, San Diego, CA, USA, 2012, pp. 1–6
- [3] Hatziargyriou, N., Asano, H., Iravani, R., et al.: 'Microgrids', IEEE Power and Energy Magazine, 2007, 5, (4), pp. 78–94
- [4] Piagi, P., Lasseter, R.H.: 'Autonomous control of microgrids'. IEEE Power Eng. Soc. General Meeting, Montreal, QC, 2006
 [5] Katiraei, F., Iravani, R., Hatziargyriou, N., et al.: 'Microgrids management',
- [5] Katiraei, F., Iravani, R., Hatziargyriou, N., et al.: Microgrids management IEEE Power and Energy Magazine, 2008, 6, (3), pp. 54–65
- [6] Ghaffarzadeh, H., Stone, C., Mehrizi-Sani, A.: 'Predictive set point modulation to mitigate transients in lightly damped balanced and unbalanced systems', *IEEE Trans. Power Syst.*, 2017, 32, (2), pp. 1041–1049
- Kahrobaeian, A., Mohamed, Y.A.I.: 'Suppression of interaction dynamics in DG converter-based microgrids via robust system-oriented control approach', *IEEE Trans. Smart Grid*, 2012, 3, (4), pp. 1800–1811
 Davari, M., Mohamed, Y.A.I.: 'Robust multi-objective control of VSC-based
- [8] Davari, M., Mohamed, Y.A.I.: 'Robust multi-objective control of VSC-based DC-voltage power port in hybrid AC/DC multi-terminal micro-grids', *IEEE Trans. Smart Grid*, 2013, 4, (3), pp. 1597–1612
- [9] Leon, A.E., Maurico, J.M., Solsona, J.A., et al.: 'Adaptive control strategy for VSC-based systems under unbalanced network conditions', *IEEE Trans. Smart Grid*, 2010, 1, (3), pp. 311–319
- [10] Liu, C., Hsu, Y.: 'Design of a self-tuning PI controller for a STATCOM using particle swarm optimization', *IEEE Trans. Ind. Electron.*, 2010, 57, (2), pp. 702–715
- [11] Bevrani, H., Habibi, F., Babahajyani, P., et al.: 'Intelligent frequency control in an AC microgrid: online PSO-based fuzzy tuning approach', *IEEE Trans.* Smart Grid, 2012, 3, (4), pp. 1935–1944
- [12] Hasanien, H.M., Matar, M.: 'A fuzzy logic controller for autonomous operation of a voltage source converter-based distributed generation system', *IEEE Trans. Smart Grid*, 2015, 6, (1), pp. 158–165
 [13] Bahrani, B., Karimi, A., Rey, B., et al.: 'Decoupled dq-current control of grid-
- [13] Bahrani, B., Karimi, A., Rey, B., et al.: 'Decoupled dq-current control of gridtied voltage source converters using nonparametric models', *IEEE Trans. Ind. Electron.*, 2013, 60, (4), pp. 1356–1366
- Electron., 2013, **60**, (4), pp. 1356–1366
 [14] Arif, J., Ray, S., Chaudhuri, B.: 'Multivariable self-tuning feedback linearization controller for power oscillation damping', *IEEE Trans. Control Syst. Technol.*, 2014, **22**, (4), pp. 1519–1526
- [15] Freijedo, F.D., Vidal, A., Yepes, A.G., et al.: 'Tuning of synchronous-frame PI current controllers in grid-connected converters operating at a low sampling rate by MIMO root locus', *IEEE Trans. Ind. Electron.*, 2015, 62, (8), pp. 5006–5017
- [16] Chen, J., Jiang, L., Yao, W., et al.: 'Perturbation estimation based nonlinear adaptive control of a full-rated converter wind turbine for fault ride-through capability enhancement', *IEEE Trans. Smart Grid*, 2014, **29**, (6), pp. 2733–2743
- [17] Li, H., Li, F., Xu, Y., et al.: 'Adaptive voltage control with distributed energy resources: algorithm, theoretical analysis, simulation, and field test verification', *IEEE Trans. Power Syst.*, 2010, 25, (3), pp. 1638–1647
- [18] Mehrizi-Sani, A., Iravani, R.: 'Online set point adjustment for trajectory shaping in microgrid applications', *IEEE Trans. Power Syst.*, 2012, 27, (1), pp. 216–223
- [19] Mehrizi-Sani, A., Iravani, R.: 'Online set point modulation to enhance microgrid dynamic response: theoretical foundation', *IEEE Trans. Power Syst.*, 2012, 27, (4), pp. 2167–2174
- [20] Stone, C., Mehrizi-Sani, A.: 'Improved dynamic response for LCC-based HVDC systems'. 2013 EPRI HVDC & FACTS Conf., Palo Alto, CA, 2013

- [21] Mehrizi-Sani, A., Iravani, R.: 'Potential-function based control of a microgrid in islanded and grid-connected modes', *IEEE Trans. Power Syst.*, 2010, 25, (4) np. 1883–1891
- (4), pp. 1883–1891

 [22] Ghaffarzadeh, H., Mehrizi-Sani, A.: 'Predictive set point modulation to mitigate transients in power systems with a multiple-input-multiple-output control system'. IEEE Innovative Smart Grid Technol. Conf. (ISGT), Minneapolis, MN, USA, 2016
- [23] Ghaffarzadeh, H., Mehrizi-Sani, A.: 'Predictive set point modulation technique to enhance the dynamic response of a power system'. IEEE Appl. Power Electron. Conf. (APEC), Tampa, FL, USA, 2017
 [24] Schilders, W.H., van der Vorst, H.A., Rommes, J.: 'Model order reduction:
- [24] Schilders, W.H., van der Vorst, H.A., Rommes, J.: 'Model order reduction: theory, research aspects and applications' (Springer, Berlin Heidelberg, Germany, 2008)
- [25] Koksal, M.E., Yakar, A.: 'Decomposition of third order linear time-varying system into its second and first order commutative pairs', CoRR, 2017, 38, pp. 4446–4464
- [26] Tabesh, A., Iravani, R.: 'Multivariable dynamic model and robust control of a voltage-source converter for power system applications', *IEEE Trans. Power Del.*, 2009, 24, (1), pp. 462–471
- [27] CIGRE Working Group C6.04.02: 'Benchmark systems for network integration of renewable and distributed energy resources', 2013